Detection and Classification of Pole-like Objects from Mobile Laser Scanning Data of Urban Environments

Hiroki YOKOYAMA[1], Hiroaki DATE[1], Satoshi KANAI[1] and Hiroshi TAKEDA[2]

[1] Graduate School of Information Science and Technology, Hokkaido University, Japan
h_yokoyama@sdm.ssi.ist.hokudai.ac.jp, (hdate, kanai)@ssi.ist.hokudai.ac.jp
[2] Kokusai Kogyo Co., Ltd, Japan, htake@kkc.co.jp

Abstract:
The Mobile Laser Scanning (MLS) system can acquire point clouds of urban environments including roads, buildings, trees, lamp posts etc. and enables effective mapping of them. With the spread of the MLS system, the demands for the management of roads and facilities using MLS point clouds have increased. Especially, pole-like objects (PLOs) such as lamp posts, utility poles, street signs etc. are in high demand as facilities to be managed. We propose a method for detecting PLOs from MLS point clouds and classifying them into three classes: utility poles, lamp posts, and street signs. Our detection method is based on the feature extraction using point classification by Principal Component Analysis (PCA). On the other hand, our classification method is based on not only shape features of the PLOs, but also context features which are derived from the surrounding PLOs distributions. In order to evaluate the accuracy of PLOs detection and classification through our method, we applied our method to MLS point clouds of urban environments.

Keywords: Mobile Laser Scanning, Point Cloud, Pole-like Object, Object Recognition, Object Detection, Object Classification

1. Introduction

With the development of inexpensive and high accuracy laser scanner devices, the Mobile Laser Scanning (MLS) system which is a vehicle mounted with these devices, GPS, INS, cameras, etc. has been widely used. The MLS point clouds can be useful not only for building and city modeling, but also for managing various facilities in urban environments. In particular, pole-like objects (PLOs) such as utility poles, lamp posts street signs, and etc. are in high demand as facilities to be managed, and it is required to recognize them from urban MLS point clouds. However, manually recognizing these PLOs from large point clouds data requires a great deal of time and cost. Therefore, for efficient management of facilities, it is necessary to automatically recognize PLOs from MLS point clouds.

Much research on PLOs detection and classification from MLS point clouds has been conducted. Existing methods are based on machine learning [3][6], the arrangement and position of measurement points [7][8], or the knowledge according to the PLO [1][10]. These methods have some problems, such as they require a lot of training data, they cannot recognize PLOs with different radii and tilt angles, and they are difficult to classify only using the shape features.

In this paper, we propose an algorithm to automatically detect PLOs from MLS point clouds and to classify them into three classes: utility poles, lamp posts, and street signs (Fig.1). Our detection method is based on Laplacian smoothing using the k-nearest neighbors graph, Principal Component Analysis (PCA) for recognizing points on the PLOs, and thresholding for the degree of PLOs (A-1). By using smoothing and PCA, robust detection of the PLOs with various radii and tilt angles is realized. Our classification method is based on not only shape features of the PLOs, but also context features which are calculated from the surrounding PLOs distributions (A-2). According to the shape features, we focused on the height, number of the parts segments, and parts structure types of the PLO. However, in some cases it is difficult to classify PLOs only using the shape features due to the similarity of the shape of the specific PLOs. By using the context features, robust classification is realized.

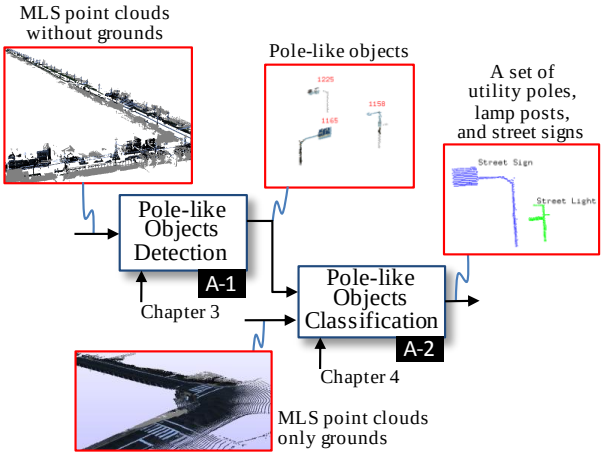

Figure 1 Proposed PLOs Detection and Classification method

Details of the existing method for PLOs detection and

classification are described in chapter 2. Details of the proposed PLO detection and classification method are described in chapter 3 and chapter 4 respectively, and the results of our method are described in chapter 5.

2. Related Works

Existing research on automatically detecting or classifying objects, including PLOs, are introduced in this chapter.

Based on machine learning, Golovinskiy et al. propose a method to classify various objects such as cars, streetlights, trees, fire hydrant, and etc. from the combination of MLS and ALS point clouds [3]. A major feature of their method is high precision segmentation by the graph cut algorithm. To classify objects, they input feature quantities of objects into the Support Vector Machine (SVM). As learning data, they used a part of the input data which are classified manually. In order to increase the recognition rate, a sufficient amount of learning data must be required. They also indicated that the better shape descriptors and classifiers are required for better results. As a similar method using machine learning, Lai et al. attempted to classify objects in MLS point clouds by using a lot of 3D data that exists on World Wide Web as learning data [6]. In the learning method, sufficient training data based on input point clouds is necessary for suitable learning.

Based on the arrangement and position of measurement points, Manandhar et al. detected vertical poles from MLS point clouds [8]. In their research, the MLS point clouds consisted of vertical scan lines and vertical poles by extracting vertical line segments from individual scan lines. Their detection method was limited to the extraction of the vertical poles. Due to this limit, the method cannot detect tilted poles and is not applicable to arbitrary point clouds. Lehtomaki et al. extracted sweeps that were expected to be measured PLOs from MLS point clouds [7]. Then they found another sweep either below the current sweep or above, and made them a cluster. However the method cannot detect PLOs with a specific radii and limited point densities.

Based on the knowledge, Lam et al. detected PLOs from MLS point clouds, and classified them into lamp posts and utility poles [1]. Their detection method was devised based on the condition that PLOs are perpendicular to the road plane. Their classification method relied on the branch of the lamp post. However, they mentioned that some utility poles also have structure that extends from the vertical column, where the power line is attached. In such condition, it was difficult to classify the PLOs. Pu et al. detected PLOs from MLS point clouds, and classified them into bare poles, trees, traffic signs, and other poles [10]. In their classification method, the straight pole (supporter) of the PLO was removed first. When remaining point cloud was non-planar, the PLO was classified as trees. When the remaining point cloud was planar, the PLO is classified as traffic sign if the shape was rectangular or

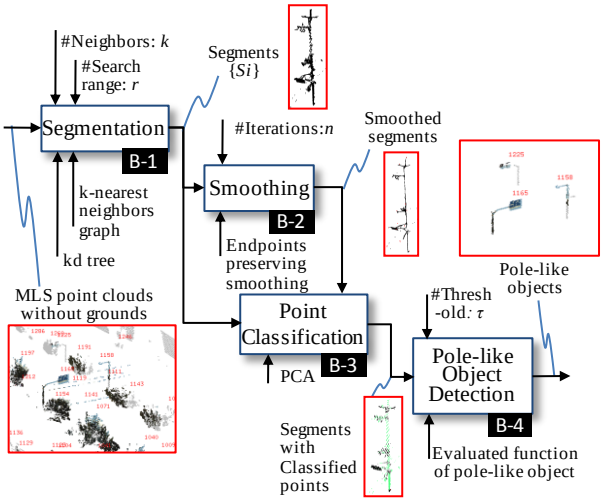

Figure 2 PLOs Detection Method

circle. If no points remained, the PLO was classified as bare pole.

In this paper, we propose a robust detection method of the PLOs with arbitrary tilt angles and radii from MLS point clouds without learning data, by using smoothing and PCA. Additionally, we propose a robust classification of the PLOs by using the shape features and context features.

3. Pole-like Objects Detection Method

3.1 Overview of the Method

The proposed algorithm is shown in Fig.2. In the method, we assume that ground points are already removed from given point clouds. The algorithm of our method consists of four steps. First, the input point clouds are segmented, as the result the points estimated on each object are grouped (B-1). Second, smoothing is applied to each segment (B-2). Third, each point is classified into the points on the PLOs, on the planar objects, and on other objects (B-3). Finally, the degree of the PLOs of each segment is evaluated, and the segments of the PLO are extracted by thresholding (B-4).

3.2 Segmentation

Many segmentation techniques of point clouds have already existed ([2], [9], and [11]). In our implementation, we adopt the simple segmentation method by connecting the nearest neighbor points. As a result, the segment is composed of the point set of the connected k-nearest neighbors graph. The graph is generated to sequentially generate an edge among the k-nearest neighbors between the point i and points included in a sphere with a radius r centered at point i. Even if the neighbors included in the sphere are less than k, we do not expand the radius r. In our experiment, k=15, r=0.5m.

3.3 Endpoint Preserving Laplacian Smoothing

The robust extraction of points on PLOs by PCA described in next section is difficult because of the measurement noises, the bias of the point distributions,

and the differences of the PLO radius. Therefore, to improve the classification rate of the points on the PLOs by PCA, endpoint preserving Laplacian smoothing is applied to the k-nearest neighbors graph in our method.

Generally, smoothing is applied for the purpose of removing the noise of the measurement data. On the other hand, recently, smoothing is used for other purposes. For example, some methods of skeleton extraction from point clouds have been proposed [4]. The purpose of their research is to extract the skeletons of wire-objects, and the recognition of the objects is not focused on.

In our method, smoothing is applied to the MLS point clouds in order to improve the classification rate of the points on the PLOs by the PCA and to distinguish points on the PLOs from the ones on the planar objects, and the others. We focus on the exaggeration and the degeneration of the object shape features based on Laplacian smoothing which is an operation that moves each point to the centres of the neighbours. Laplacian smoothing makes the PLOs into a thin pole shapes through shape degeneration. As the result, the point distributions of the PLOs come to be degenerated into a one dimensional distribution (Fig.3). In addition, measurement noises are removed. Therefore, applying the Laplacian smoothing to the scan data raises the classification rate of the PLO points by the PCA. Laplacian smoothing is done by applying Eq.(1):

$$\mathbf{p}_i' = \mathbf{p}_i + \lambda \Delta \mathbf{p}_i \quad (1)$$

where $\mathbf{p}_i'$ is the position of point i after smoothing, $\mathbf{p}_i$ is the position of point i, λ is the smoothing strength ($0 \leq \lambda \leq 1$), $\Delta \mathbf{p}_i$ is the Laplacian, and it is given by the Eq.(2):

$$\Delta \mathbf{p}_i = \sum_{j \in i^*} \omega_{ij} \left(\mathbf{p}_j - \mathbf{p}_i \right) \quad (2)$$

where ω_{ij} is the positive weight ($\sum_{j \in i^*} \omega_{ij} = 1$), i^* is a set of the neighbors of point i. The point clouds of PLOs with various radii can be degenerated into a one dimensional distribution by iteratively applying Eq.(1), and then PLOs with various radii can be detected.

However, Laplacian smoothing has the problem that the branching structures of the PLOs are lost. This causes the decrease of the classification rate in the following PLO classification step. To solve this problem, we propose the endpoints preserving Laplacian smoothing, which controls displacements during smoothing according to the distribution of the neighbors of a point. At the endpoint, the neighbors are distributed in one direction. On the other hand, the neighbors are distributed in all directions at the inner point. From this observation, the displacements during smoothing are controlled so as to preserve the endpoints according to the distribution of the neighbors. We evaluate whether point i is the endpoint or not using Eq.(3):

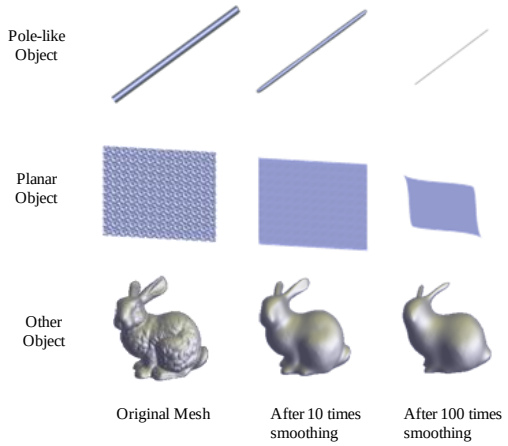

Figure 3 Examples of degenerated objects in mesh model by smoothing

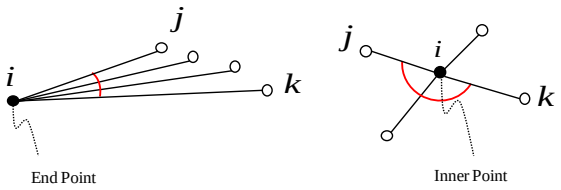

Figure 4 Neighbors' distribution at the endpoint and the inner point

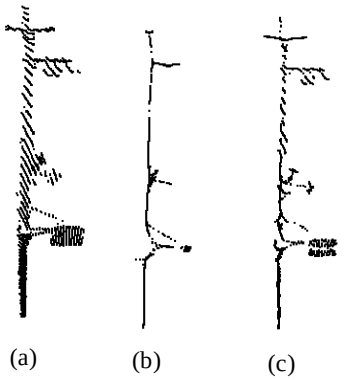

(a) input point clouds of utility pole
(b) after Laplacian smoothing
(c) after endpoint preserving Laplacian smoothing (iteration times n=40)
Figure 5 Comparative result of smoothing

$$e(i) = \frac{1}{|V_i| \times \pi} \sum_{(j,k) \in V_i} angle(j,i,k) \quad (3)$$

where i^* is a set of neighbors of point i, $V_i = \{(j,k) \mid j,k \in i^*, j \neq k\}$, $angle(j,i,k)$ is the angle of j,i,k. If the point i is the endpoint, $angle(j,i,k)$ is small (Fig.4 left), then the $e(i)$ becomes small. On the other hand, if the point i is far from the endpoint, some $angle(j,i,k)$ are large (Fig.4 right), then $e(i)$ becomes large.

Displacements in smoothing can be controlled by using the smoothing strength λ. Additionally in order to

reduce influences of the distant points during smoothing, we use weight ω_{ij} which is in inverse proportion to the distance between points. Endpoints preserving Laplacian smoothing is done by the equations (4), (5), and (6):

$$\mathbf{p}_i' = (1-\lambda)\mathbf{p}_i + \lambda \sum_{j \in i^*} \omega_{ij} \mathbf{p}_j , \quad (4)$$

$$\lambda = e(i) , \quad (5)$$

$$\omega_{ij} = \frac{\left|\mathbf{p}_j - \mathbf{p}_i\right|^{-1}}{\sum_{j \in i^*} \left|\mathbf{p}_j - \mathbf{p}_i\right|^{-1}} . \quad (6)$$

Figure 5 shows the comparative result of the Laplacian smoothing and endpoint preserving Laplacian smoothing for the same utility pole. Fig.5(a) shows the input point clouds of the utility pole. Fig.5(b) and Fig.5(c) show the results of the Laplacian smoothing and endpoint preserving Laplacian smoothing respectively. After the endpoint preserving Laplacian smoothing, the branching structures still remain. During iterating smoothing, the distribution of the points on the PLOs with various radii becomes one dimension. In our experiment, the number of iterations of the smoothing is 40.

3.4 Point Classification

Each point is classified into three types which are the points on the PLO, the points on the planar object, and the others. The local point distributions are evaluated by calculating eigenvalues and eigenvectors of the variance-covariance matrix related to the point i and its neighbors. The variance-covariance matrix $\mathbf{M}_i$ of the point i is shown in Eq.(7):

$$\mathbf{M}_i = \frac{1}{\left|i^*\right|} \sum_{j \in i^*} \left(\mathbf{p}_j - \bar{\mathbf{p}}_i\right)\left(\mathbf{p}_j - \bar{\mathbf{p}}_i\right)^T , \quad (7)$$

where $\mathbf{p}_i$ is the position of point i, i^* is a set of the neighbor points of point i, $\bar{\mathbf{p}}_i$ is the barycenter of i^*. We denote eigenvalues of the $\mathbf{M}_i$ by λ_1^i, λ_2^i, and λ_3^i ($\lambda_1^i \geq \lambda_2^i \geq \lambda_3^i$) and the corresponding unit eigenvectors by $\mathbf{e}_1^i$, $\mathbf{e}_2^i$, and $\mathbf{e}_3^i$ respectively. The local distribution of neighbors of point i is figured out by the magnitude relation of the eigenvalues.

When point i is on the PLO, the maximum eigenvalue λ_1^i is very large compared with other eigenvalues λ_2^i, λ_3^i, and the eigenvector $\mathbf{e}_1^i$ represents the axial direction of the PLOs. On the other hand, when point i is on the planar object, λ_1^i and λ_2^i become relatively large compared with λ_3^i. When point i is on the other object, there are not so many differences between the three eigenvalues.

In order to investigate the magnitude relation of eigenvalues, we compute the dimensionality feature d_i using Eq.(8) [12]:

$$d_i = \arg_{j \in \{1,2,3\}} \max S_j^i , \quad (8)$$

where S_1^i, S_2^i, and S_3^i are the distribution features, and

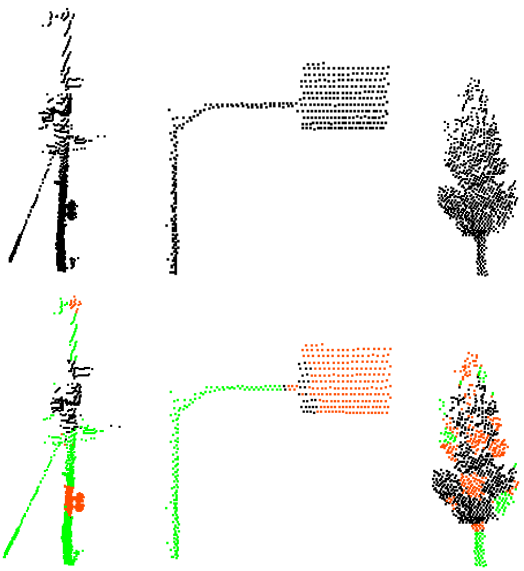

(a) utility pole (b) street sign (c) tree

(green: points on the PLO objects, orange: points on the planer objects, black: points on others)

Figure 6 Results of the point classification

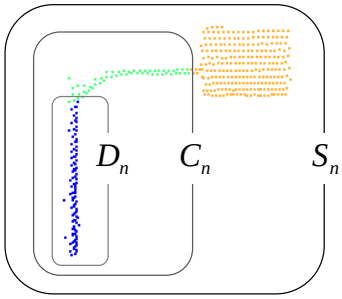

(green: points on the PLO objects, orange: points on the planer objects, blue: points whose neighbors are distributed vertically)

Figure 7 Example of the point clouds of a street sign

defined by Eq.(9):

$$S_1^i = \lambda_1^i - \alpha\lambda_2^i, \quad S_2^i = \lambda_2^i - \lambda_3^i, \quad S_3^i = \beta\lambda_3^i , \quad (9)$$

where α, β are the adjustment coefficient. When point i is on the PLO or planar object or other object, d_i becomes 1, 2, and 3 respectively. Figure 6 shows the results of the point classification. Fig.6(a)-(c) shows the utility pole, street sign, and tree respectively. The top row represents the input point clouds. The bottom row represents the point classification results after smoothing. In our experiment, α and β are set to 10, 100 respectively.

3.5 PLOs Detection

Finally by evaluating the geometric properties and classified points of the segments, each segment is classified into PLO and others. As the minimum requirement for the PLO, we assume that the height of

the segment is more than 2m which is higher than average human height, and that the number of points of the segment is over 50. Hence, the segments which do not satisfy these conditions are recognized as other type objects. In addition, the segment in which over 70% of points are the ones on the other objects is recognized as other objects, because the PLOs we intended consist of poles and plane surfaces. For each remaining segment, the degree of the PLOs is evaluated by Eq.(10):

$$f_n = \left(w_1 \frac{|C_n|}{|S_n|} + w_2 \frac{|D_n|}{|C_n|} \right) \times \frac{100}{w_1 + w_2}, \qquad (10)$$

where w_1, w_2 are weights. S_n is a set of points of segment n. C_n is a set of points on the PLOs, and included in S_n. D_n is a set of points that have almost vertical $\mathbf{e}_1^i$, and included in C_n. In our experiment, w_1=1.0, w_2=2.0.

An example of the sets of points S_n, C_n, and D_n for a street sign is shown in Fig.7. The first term of Eq.(10) represents the ratio of the points on the PLOs in the segment. The second term of Eq.(10) represents the ratio of the points whose neighbors are distributed vertically in the points on the PLOs. The degree of the PLO for each segment is evaluated by the weighted sum of the two terms. Figure 8 shows the histogram of the value f_n about various objects in MLS point clouds. The value f_n becomes lager for the almost segments of PLOs. In our experiment, because it was observed that the segments of the PLO had f_n over about 45, τ is set to 45. Finally, the segments which have f_n larger than the threshold are recognized as PLOs.

4. Pole-like Objects Classification Method

4.1 Overview of the Classification Method

The proposed classification algorithm is shown in Fig.9. The algorithm of our method consists of four steps. First, the supporters of the PLOs and attached parts to the supporters are segmented (B-5). As the result, the points on each attached part are grouped. Second, the membership values are calculated using the membership functions of the utility pole, lamp post, and street sign, which are defined by the height, the number of the attached parts, and the structure type of the attached parts of the PLO (B-6). Third, the context features using the relative positions of surrounding PLOs are calculated (B-7). Finally, using the membership values and context features, the PLOs are classified into utility poles, lamp posts, and street signs (B-8).

4.2 Segmentation of Each PLO

In each PLO, the attached objects (parts) to the supporters can be the important classification cues. Therefore the supporters and attached parts are recognized from the point clouds of PLO.

In this step, the results of the smoothing and the point classification are used (described in section 3.3 and 3.4 respectively). Line RANSAC is applied to the points

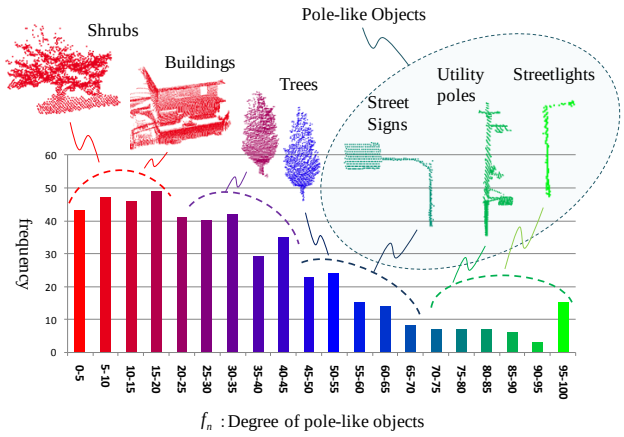

Figure 8 Histogram of f_n, and objects in MLS point clouds

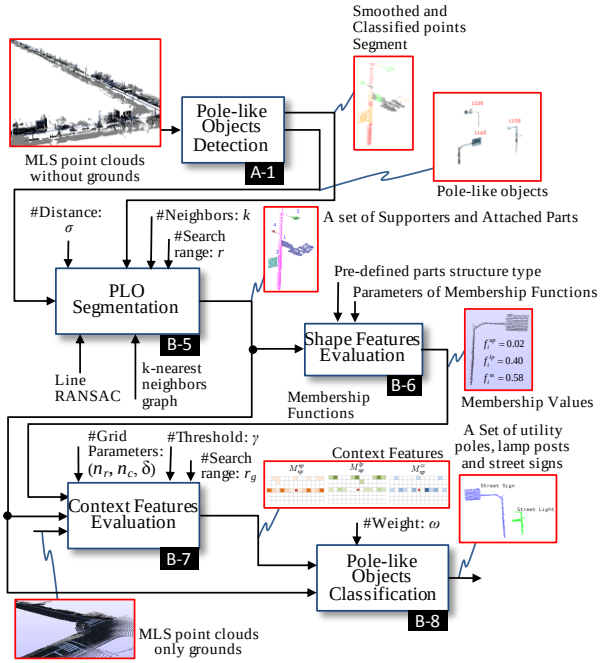

Figure 9 PLOs Classification Method

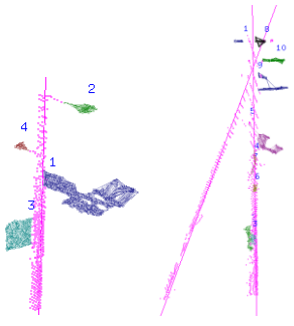

(a) (b)

(a): lamp post with signals
(b): utility pole composed of two supporters
(pink points: points on the supporter of PLOs, pink line: fitting line of line RANSAC, label number: attached part segment number)

Figure 10 Results of the segmentation of the supporters and attached parts

whose neighbors are distributed vertically (that is, the points that have possibility to being on the supporters, as shown in D_n of Fig.7). The points which lie within the distance σ from the fitting line are recognized as the points on the supporter of the PLO regardless of its dimensionality feature. Figure 10 shows the results of the supporter recognition. This process is repeated until the number of points which are fitted to the line becomes less than δ_1 in order to recognize more than two supporters. Since the distances from the fitting line are calculated using points after smoothing, robust supporter recognition of the PLOs with various radii is realized.

In order to analyze each attached part of the PLO, the segment for each part is extracted. First, k-nearest neighbors graph is created for the points on the PLO without the points on the supporters. Then, each connected component is recognized as a part segment. Fig.10 shows the result of the attached part segmentation. In our experiment, σ and δ_1 are set to σ=0.20m and δ_1=50 respectively.

4.3 Shape Features Evaluation

Each attached part structure can be the important feature for classifying the PLOs. The point set includes more than δ_2 (δ_2=10) and they have the same dimensionality feature d_i (calculated in section 3.4) on the part segment are extracted. The point set is classified into pole elements, plane elements, and volume elements if d_i of points in the point set is 1, 2, and 3 respectively. Each attached part is classified into pre-defined eight types of structures shown in Fig.11 according to the kind of elements contained in the part.

In our research, PLOs are classified into utility poles, lamp posts, and street signs. In many cases, PLOs have standard heights, therefore the height of PLOs become the feature for classifying. Additionally, in many cases, the utility poles have a lot of attached parts from their roles. On the other hand, the lamp posts and street signs have few attached parts. Therefore the number of the attached parts of the PLOs becomes the feature for classifying. Furthermore, the structures of the attached parts of PLOs are limited to some extent for every class, therefore the attached parts types become the feature for classifying.

The membership values of the utility pole (*up*), lamp post (*lp*), and street sign (*ss*) are evaluated by Eq.(11) using the height, the number of the attached parts, and the structure type of the attached parts of the PLOs:

$$f_i^{class} = h_i^{class}(S_h) + g_i^{class}(S_{pn}) + \frac{c_i^{class}(S_{pt})}{S_{pn}} \quad (11)$$

where $class \in \{up, lp, ss\}$, and

$$h_i^{class}(S_h) = \begin{cases} 1.0 & h_{\min} \le S_h \le h_{\max} \\ 0.0 & otherwise \end{cases},$$

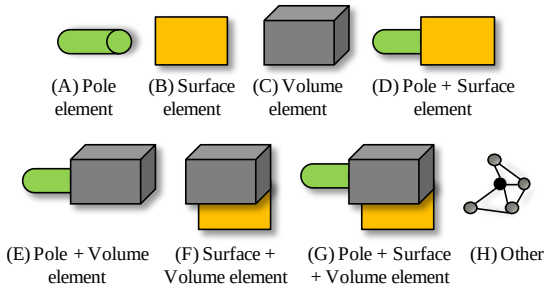

Figure 11 Pre-defined part structure types

Table 1 Parameters of the membership functions

	$h_{\min}$[m]	$h_{\max}$[m]	a	b	T
f_i^{up}	6.5	15.0	0.1	0.0	(C,H)
f_i^{lp}	3.0	12.0	-0.2	1.0	(A,E)
f_i^{ss}	2.0	6.5	-0.3	0.9	(B,D,F,G)

$$g_i^{class}(S_{pn}) = \begin{cases} 1.0 & aS_{pn} + b > 1.0 \\ 0.0 & aS_{pn} + b < 0.0 \\ aS_{pn} + b & otherwise \end{cases}.$$

Where f_i^{up}, f_i^{lp}, and f_i^{ss} are the membership values of the utility pole, lamp post, and street sign respectively. Table 1 shows the parameters of each membership function. S_h, S_{pn}, and S_{pt} are the height of the PLO segment, the number of the part segment in PLO segment, and the set of the attached parts types in the PLO segment respectively. $c_i^{class}(S_{pt})$ is a function that counts the number of the attached parts included in the parts structure types in T shown in Table 1. If there is no attached part, S_{pt} is 0. Parameters in Table 1 were set based on the observation of acquired MLS point clouds and catalog specification of the products. These three membership values are normalized.

However, it is difficult to accurately classify PLOs only using the membership values due to the similarity of the shape of the specific PLOs. To solve the problem, we introduce the context features.

4.4 Context Features Evaluation

The relative position of a PLO to its surrounding PLOs is a useful cue for classification. Utility poles, for example, are found on side of a road at regular intervals. We introduce autocorrelation as the context feature.

The procedure of context features evaluation consists of four steps.

i) The regular 2D-grid G_i centered at the position of the supporter of the PLO segment S_i is generated. Each cell of the grid is a square, and the length of its side is δ[m]. The numbers of the rows and the columns are n_r and n_c respectively. Each grid direction is adjusted to the direction of the nearest road of the S_i. To find the direction of the road, PCA is applied to road point clouds within the wide range (sphere with radius r_g centered at the S_i). The nearest road direction of the PLO is calculated as the eigenvector $\mathbf{e}_1$ corresponding

to the max eigenvalue λ_1. In our experiment, n_r=6, n_c=20, δ=6.0m, and r_g=20m.

ii) For all PLO segment S_j on G_i, its membership values f_j^{up},f_j^{lp}, and f_j^{ss} are accumulated to the cell including the S_j. As a result, as shown in Fig.12, three surrounding PLOs distribution maps (matrices) $\mathbf{m}_i^{up}$, $\mathbf{m}_i^{lp}$, and $\mathbf{m}_i^{ss}$ which have the surrounding PLOs membership values f_j^{up},f_j^{lp}, and f_j^{ss} at each cells respectively are generated.

iii) Define U, V, and W as the sets of utility poles, lamp posts, and street sings which can be clearly classified only using the membership values. In our experiment, $U=\{S_k \mid f_k^{up} > \gamma\}$,$V=\{S_k \mid f_k^{lp} > \gamma\}$,$W=\{S_k \mid f_k^{ss} > \gamma\}$, where γ is a threshold for membership values. According to the U, V, and W, the average surrounding PLOs distribution maps (matrices) $\overline{\mathbf{m}}_{true\_class}^{up}$, $\overline{\mathbf{m}}_{true\_class}^{lp}$, and $\overline{\mathbf{m}}_{true\_class}^{ss}$ ($true\_class \in \{up,lp,ss\}$) are generated using the Eq.(12):

$$\begin{cases} \overline{\mathbf{m}}_{up}^{class} = \dfrac{1}{|U|}\sum_{i\in U}\mathbf{m}_i^{class} \\ \overline{\mathbf{m}}_{lp}^{class} = \dfrac{1}{|V|}\sum_{i\in V}\mathbf{m}_i^{class} \\ \overline{\mathbf{m}}_{ss}^{class} = \dfrac{1}{|W|}\sum_{i\in W}\mathbf{m}_i^{class} \end{cases}, class \in \{up,lp,ss\} \quad (12)$$

The value of cell of $\overline{\mathbf{m}}_b^a$ is the probability of existence of the object of the class 'a' when center object of the grid belongs to the class 'b'. In our experiment, γ=0.60.

iv) The similarities between $\mathbf{m}_i^{class}$ and $\overline{\mathbf{m}}_{true\_class}^{class}$ are defined as the context feature, and it is evaluated by Eq.(13):

$$\begin{cases} \hat{f}_i^{up} = \sum_{class\in\{up,lp,ss\}} \left\langle \mathbf{m}_i^{class}, \overline{\mathbf{m}}_{up}^{class} \right\rangle \\ \hat{f}_i^{lp} = \sum_{class\in\{up,lp,ss\}} \left\langle \mathbf{m}_i^{class}, \overline{\mathbf{m}}_{lp}^{class} \right\rangle \\ \hat{f}_i^{ss} = \sum_{class\in\{up,lp,ss\}} \left\langle \mathbf{m}_i^{class}, \overline{\mathbf{m}}_{ss}^{class} \right\rangle \end{cases} \quad (13)$$

where $\hat{f}_j^{up}$, $\hat{f}_j^{lp}$, and $\hat{f}_j^{ss}$ are the context features of the utility pole, lamp post, and street sign respectively. The <x, y> is the sum of products of the values of each corresponding cell of x and y. The range of the context features are adjusted to [0,1] by $\hat{f}_i^{class} = \hat{f}_i^{class} / \max_{class\in\{up,lp,ss\}} \hat{f}_i^{class}$.

4.5 PLOs Classification

Finally, the PLOs are classified into utility poles, lamp posts, and street signs, using the membership values and context features by the Eq.(14):

$$S_i^{class} = \arg_{class\in\{up,lp,ss\}} \max\left(f_i^{class} + \omega \hat{f}_i^{class}\right), \quad (14)$$

where ω represents the positive weight, and in our experiment, ω=0.25.

5. Results

5.1 Data and Measurement System

Point Clouds of urban environment acquired by MLS system shown in Table 2 were used in our experiments

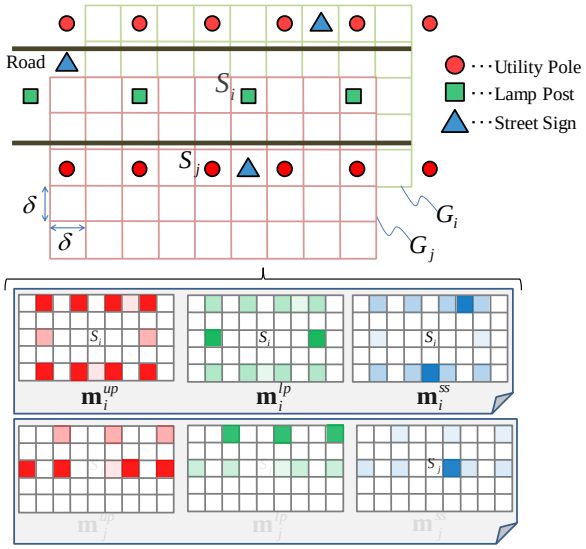

Colors on the maps represent the utility pole (red), lamp post (green) and street sign (blue) respectively, indicating that membership values are so big that they are deep-colored.

Figure 12 Surrounding PLOs distribution map centered at the PLO segment S_i and S_j

Table 2 Data used in the article

Data	Measurement Place	Number of Point (million)	Measurement System
I	Kyoto, Japan	2.5	MMS-X
II	Kyoto, Japan	1.0	MMS-X

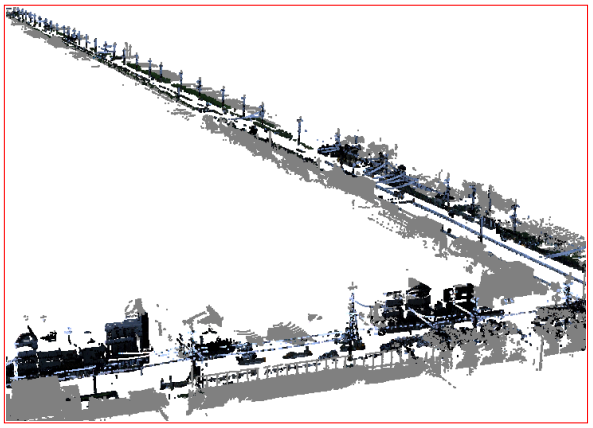

(a) input data I

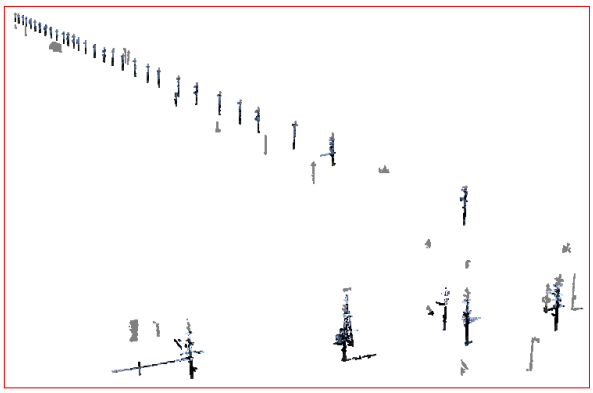

(b) output in our PLOs detection method

Figure 13 Result of the PLOs detection

[5]. As described in section 3.1, the ground points were removed manually from the given data. In our methods, each parameter in the algorithm is determined based on the experiments. Our method is implemented using standard PC (OS: Windows7 64bit, CPU: Intel Core i7 3.0 GHz, RAM: 6GB).

5.2 PLOs Detection Result

Figure 13 shows the result of the PLOs detection by our method. In Fig.13(a), there are a lot of various objects such as trees, buildings, cars, and PLOs. In Fig.13(b), the PLOs such as lamp posts and utility poles are detected. However, some other objects such as trees are included. The detection accuracy of the PLOs is shown in Table 3. The number of correct PLOs [B] was manually verified by using the photograph. [G] is the number of objects which were recognized as PLOs though they are not the PLOs. The average accuracy of the PLO detection is 69.7% for correct PLOs. On the other hand, the average accuracy of PLOs detection is 92.2% for correctly created PLOs.

Our detection method is designed for correctly segmented point clouds, therefore detection failed for the incorrect segments as shown in Fig.14. The [F] in Table 3 shows our method works well for the correctly created segments. In the future, we will apply an appropriate segmentation method such as [2] to the inputs and evaluate the detection rate. Processing times of the PLOs detection are shown in Table 4.

5.3 PLOs Classification Result

Table 5 shows the accuracy of the PLOs classification only using the membership values. From the table, the average accuracy of PLOs classification is 66.7% for PLOs which are correctly segmented in the PLOs detection algorithm. On the other hand, Table 6 shows the accuracy of the PLOs classification using both membership values and context features. From the table, the accuracy of classification related to the utility pole is improved. Here it should be noted that the context features could be calculated properly if there is regularity in the distribution of PLOs. In our experiment, because such regularity is seen in Data I, the classification accuracy was improved. Figure 15 shows the results of the PLOs classification of Data I. Top of the figure shows the result only using the membership values, on the other hand, the bottom of the figure shows the result using not only the membership values but also context features. From comparison of the results, context features work well. Processing times of the PLOs classification are shown in Table 7.

6. Conclusion

In this article, we developed an algorithm for automatically detecting PLOs with tilt angles and various radii from MLS point clouds in urban environments, and classifying them into three classes: utility poles, lamp posts, and street signs. Our detection method is based on the smoothing and principal component analysis for point clouds, and the evaluation of the degree of PLOs for the segments using the point classification result. The

Table 3 Accuracy of the PLOs detection method

Data	I	II
[A] The number of total segments satisfying the minimum requirements	209	92
[B] The number of correct PLOs	63	25
[C] The number of correctly segmented PLOs	52	17
[D] The number of correctly detected PLOs	50	15
[E] Detection Rate within correct PLOs (=[D]/[B])	79.3%	60.0%
[F] Detection Rate within correctly segmented PLOs (=[D]/[[C])	96.2%	88.2%
[G] The number of false detection	24	13

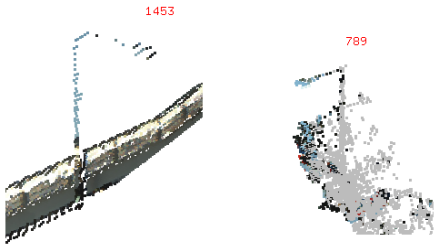

Figure 14 Undetectable PLOs by our detection method

Table 4 Running time of PLOs detection method

Processing	I	II
Creation of kd tree	17.1	5.9
Segmentation	45.7	24.6
Smoothing	28.1	13.7
Point classification	17.7	17.0
PLOs detection	0.05	0.02
Total running time of detection	108.7sec	61.2sec

Table 5 Accuracy of the PLOs classification only using the membership values*

		Algorithm				Classification Accuracy
		up	*lp*	*ss*	Total	Classification Rate
True Class	*up*	39	15	0	54	72.2%
	lp	1	7	1	9	77.8%
	ss	0	1	1	2	50.0%
	Total	40	23	2	65	66.7%

**up*, *lp*, and *ss* represent the utility pole, lamp post, and street sign respectively. The PLO segments of true class are used from [D] in Table 2.

Table 6 Accuracy of the PLOs classification using the membership values and context features*

	Classification Acuracy	
Class	using membership values only	Using membership values and context features
up	39/54 (72.2%)	44/54 (81.5%)

**lp*, and *ss* cannot be evaluated due to few samples.

PLOs detection rate was on average 92.2% for correctly segmented PLOs. Our classification method is based on shape features and context features of the PLOs. In our method, the shape feature of each PLO is calculated from the height, number of the parts segments, and parts structure types of the PLO. Context features are calculated from the surrounding PLOs distributions. By only using the membership values, the average accuracy of PLOs classification was 66.7% for PLOs which are correctly segmented in the PLOs detection algorithm. By using both membership values and context features, the accuracy of the classification was improved to 81.5% related to the utility pole.

Future works are to improve the detection and classification rate by adopting or developing an appropriate segmentation method, and to apply our method to various MLS point clouds and evaluate its performance.

Acknowledgement

We would like to thank Ishikawa Kiichiro of Waseda University for providing the MLS point clouds.

References

[1] Lam, J., Kusevic, K., Mrstik, P., Harrap, R. and Greenspan, M., 2010, Urban Scene Extraction from Mobile Ground Based LiDAR Data, 5th International Symposium on 3D Data, Processing, Visualization and Transmission.

[2] Golovinskiy, A. and Funkhouser, T., 2009a. Min-Cut Based Segmentation of Point Clouds, IEEE Workshop on Search in 3D and Vision (ICCV).

[3] Golovinskiy, A., Kim, V. and Funkhouser, T., 2009b, Shape-based Recognition of 3D Point Coluds in Urban Environments, International Conference on Computer Vision, pp2154-2146.

[4] Au, O., Tai, C., Chu, H., Cohen-Or, D. and Lee, T., 2008, Skeleton Extraction by Mesh Contraction, Proceeding of ACM SIGGRAPH, Vol.27, issue 3.

[5] Ishikawa, K., Amano, Y., Hashizume, T., Takiguchi, J. and Shimizu, S., 2009, City Space 3D Modeling using a Mobile Mapping System (in Japanese), The Society of Instrument and Control Engineers Trans. on Industrial Application, Vol.8, No.17, pp.133-139.

[6] Lai, K. and Fox, D., 2009, 3D Laser Scan Classification Using Web Data and Domain Adaptation, Robotics: Science and Systems.

[7] Lehtomaki, M., Jaakkola, A., Hyyppa, J., Kukko, A. and Kaartinen, H., 2010, Detection of Vertical Pole-Like Objects in a Road Environment Using Vehicle-Based Laser Scanning Data, Remote Sensing, Vol.2, pp.641-664.

[8] Manandhar, D. and Shibasaki, R., 2001, Feature Extraction from Range Data, Proceeding of the 22nd Asian Conference on Remote Sensing, Vol.2, pp.1113-1118.

Table 7 Running time of PLOs classification method

Processing	I	II
PLO Segmentation	6.1	6.9
Shape features evaluation	23.2	6.54
Context features evaluation	1.0	0.71
PLOs classification	0.02	0.03
Total running time of classification	30.3sec	14.2sec

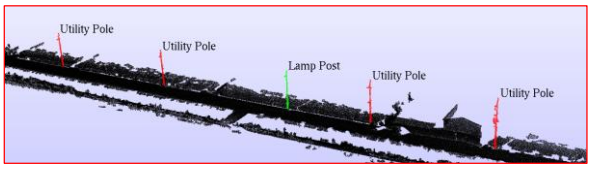

(a) result of the classification only using membership values

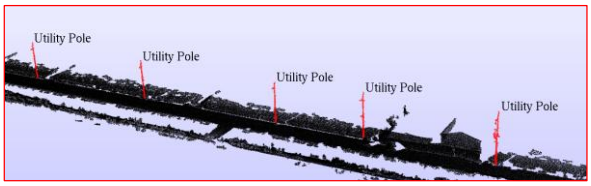

(b) result of the classification using membership values and context features

Figure 15 Effectiveness of the context features

[9] Moosmann, F., Pink, O. and Stiller, C., 2009, Segmentation of 3D Lidar Data in Non-flat Urban Environments using a Local Convexity Criterion, Proc. IEEE Intelligent Vehicles Symposium, pp.215-220.

[10] Pu, S., Rutzinger, M., Vosselman, G. and Elberink, O., S., 2011, Recognizing Basic Structures from Mobile Laser Scanning Data for Road Inventory Studies, Journal of Photogrammetry and Remote Sensing, Vol.66, issue 6, pp28-39.

[11] Wang, L. and Chu, H., 2008, Graph Theoretic Segmentation of Airborne LiDAR Data, Proc. SPIE Defense and Security Symposium, pp.69790N-1-10.

[12] Demantke, J., Mallet, C., David, N. and Vallet, B., 2011, Dimensionality Based Scale Selection in 3D Lidar Point Clouds, International Archives of Photogrammetry, Remote Sensing and Spatial Information Sciences, Laser Scanning 2011.